

Transition between the regimes is characterized by a rapid drop in frequency. The relation between the flows generated by a force and those past a circular cylinder is identified.

PACS: 47.15.Tr; 47.32.ck; 47.27.ek

Keywords: localized force; drag wake; vortex street

0. INTRODUCTION

The problem of the quantitative description of the characteristics of wakes behind bodies towed in a viscous fluid arises in a large number of applications. The characteristics of the drag wakes occurring behind bluff bodies are relatively well studied. In particular the flow around a cylinder, which is a benchmark problem in fluid mechanics, has a long history of serious investigation (see comprehensive reviews by Zdravkovitch [1] and Williamson and Govardhan [2]). Herein, we formulate an idealized problem where the wakes are generated by a spatially localized force acting on the fluid. A towed object experiences a drag force. The effect of the object on the fluid is therefore described by the force equal to the drag force in magnitude and acting in the opposite direction. Therefore, we can specify the magnitude of the force rather than the size and the details of shape of a particular object and then study the vortical wake generated by such a forcing. Although investigating the physics of bluff body wakes was our primary motivation the results were somewhat unexpected. The generalized formulation employed here leads to a wider class of flows. This fact can be understood from a simple analysis of control parameters of the problem. A single parameter, the Reynolds number which includes three dimensional parameters, namely the diameter of the cylinder d , the velocity of the stream U and the kinematic viscosity of fluid ν , suffices to characterize a flow past a circular cylinder. Our problem, however, contains one additional parameter, the magnitude of the force J . Thus, in terms of control parameters, our problem contains an extra degree of freedom. This new class of flows is of great interest from the point of view of its connection to bluff body wakes as well as from a more general fluid dynamical perspective of flows induced by a localized forcing. A simple example can

demonstrate that this class of flows includes flows which are different from a wake. An extreme case can be considered when the forcing is stationary (or translates very slowly). It is well known that such a forcing generates a vortex dipole in front of a developing jet (e.g. [3, 4]). The primary goal of this study is therefore to investigate quantitatively different regimes of the flow and to clarify its physics. The idea that translating localized force can generate flows similar to bluff body wakes for certain values of control parameters yet demonstrating other regimes as well, was first verified in the laboratory experiments [5]. In these experiments a permanent magnet was translated above the surface of the conducting fluid (salt water). A combination of the vertical component of the magnetic field with the electric current flowing in the horizontal (spanwise) direction in the fluid results in a Lorentz force on the fluid in the direction of translation of the magnet. The experiments were performed in a thin layer of fluid where the bottom boundary layer was present. Herein, we investigate similar idealized flows in a perfectly two-dimensional geometry.

1. NUMERICAL SIMULATIONS

A large number of two-dimensional numerical simulations that document the flows generated by a localized momentum source, have been performed for a wide range of governing parameters. The simulations were performed using the commercial computational fluid dynamics code Fluent 5.5.14 on the SGI Onyx 3400 computer. Fluent code was validated by the code developers using (among other problems) the benchmark problem of the flow around a circular cylinder. Further verifications were provided by other researchers who investigated cylinder wakes using Fluent software

(e.g. [6-8]). Since the wake flows investigated in this work are dynamically related to bluff body wakes the previous verifications provide a good basis for the present simulations.

Simulations reported herein were carried out using the Navier-Stokes solver such that the governing equations are of the form:

$$\frac{\partial \mathbf{u}}{\partial t} + \mathbf{u} \cdot \nabla \mathbf{u} = -\frac{1}{\rho} \nabla p + \nu \nabla^2 \mathbf{u} + \frac{1}{\rho} F(\mathbf{x}, t)$$

$$\nabla \cdot \mathbf{u} = 0$$

where \mathbf{u} , p , ρ and ν are the fluid velocity, pressure, density and kinematic viscosity. A localized force ρJ was applied to a fluid in a circle of radius a such that the force density F (force per unit area) is described by the Gaussian distribution $F = F_0 \exp(-r^2 / a^2)$ (e.g. Maxey and Patel [9]). The force was applied in the negative direction of the x-axis, against the incoming stream. The amplitude of the force F_0 was varied in our simulations. Note that a different representation of a force is usually used in order to generate a flow similar to that due to a presence of a bluff body. If the force is proportional to local value of velocity in the flow (e.g. Angot et al. [10]) it results in relaxing the velocity in the area where the force is applied to zero (similar to the Rayleigh sponge) thus satisfying the boundary conditions on the surface of a (virtual) body. We rather chose an approach where the force is independent of velocity because this corresponds to a more general formulation of a problem of flows generated by a constant force which is specified *a priori*. Besides, Gaussian distribution provides a convenient one-parameter representation of the bell-like distribution of the electromagnetic forcing which was used in our recent laboratory experiments [5]. Thus, a primary goal of this work was to study

the flows generated by such an idealized forcing rather than finding an exact distribution of force modeling a particular bluff body.

All operators in the finite-volume formulation were discretized using central-difference schemes. The temporal discretization was second-order accurate in all simulations. A computational domain of dimensions 250×75 (in units of $2a$) was used in our simulations. The domain was large enough compared to the size of the forcing area and to the width of the wake such that the effect of its boundaries on the flow can be neglected during the entire period of the flow evolution. The domain was filled with an unstructured grid consisting of 85,000 triangular elements with a minimum mesh size of 0.07. The size of the elements was smaller where the values of velocity shear in the flow were larger and smaller where the flow was approximately irrotational (Figure 1). A sensitivity study was performed prior to the main simulations where grids of similar geometry but where decreasing number of nodes were used. This study demonstrated that at the number of nodes less than approximately 45000 the results started to show some dependence on the grid size. A grid of 85000 nodes was finally chosen such that the simulations can be safely considered to be independent of the grid size. A uniform inflow of velocity U was sustained at the left wall of the domain while the outflow boundary conditions were specified at the right wall. Free-slip boundary conditions were applied at the lateral boundaries of the domain. The nondimensional time step (approximately 0.1) was chosen such that 25-30 iterations were performed during one period of vortex shedding. The same parameter choice is also considered to be optimum for the simulations of the benchmark cylinder flow. In what follows the distances are measured in units of $2a$ while time is nondimensionalized by $2a/U$.

In the experiments where the flow becomes unstable it exhibits a transient behavior before the regular vortex shedding establishes in the wake of the force. This intermediate evolution of the flow involves a formation of a vortex dipole which will be described in more detail in the following Section. This transient evolution can take a significant time. In those experiments where we were only interested in measuring the frequency of vortex shedding in the established vortex street we introduced perturbation to the flow in order to trigger the instability and to avoid the intermediate stage. Destabilizing effects occur naturally in the physical experiment. In the idealized numerical simulation the boundary conditions are symmetric and only the round-off errors and the errors due to finite difference representation of equations can eventually cause the asymmetry of the solution. Different methods are employed in numerical simulations to model the perturbations (e.g. Braza et al. [11]). An important condition is that the artificial perturbations can change the regime of the flow but cannot be the source of energy sustaining this regime. We chose to use the asymmetric perturbation of the boundary condition. A 5% difference in the velocity in the upper and lower halves of the domain was introduced at the inflow boundary for a very short period of time (a few time steps). The direct comparison of the shedding frequency for the flows with and without the perturbation showed that the values were equal. The frequency of the vortex shedding is therefore independent on the peculiarities of the initial evolution of the flow and the oscillating regime of the flow is due to natural factors rather than to the introduced perturbation. The frequency of shedding was measured using the following method. The mean value of vorticity was calculated for positive values of y along a line located perpendicular to the axis of the flow at $x = 7.5$. The vorticity was calculated at each time

step for several (5 - 10) periods of vortex shedding. The time series of the vorticity values was then analyzed using a Fourier transform to find the shedding frequency.

2. RESULTS AND INTERPRETATION

To better understand the results of the numerical simulations, it is useful to first perform a simple dimensional analysis of the control parameters involved in the problem. Consider the frequency, f , of vortex shedding which depends on a set of four dimensional quantities namely, the kinematic viscosity ν , the velocity U , the amplitude of forcing J and the size of the region where the force is applied, a . Dimensional analysis then gives

$$\frac{fU^3}{J} = \Phi\left(\frac{J}{\nu U}, \frac{J}{aU^2}\right), \quad (1)$$

where Φ is an unknown function of two dimensionless arguments. The first argument $\Pi_\nu = J/(\nu U)$ of the function Φ includes viscosity and can be considered as an analogue of the Reynolds number of the flow. The second argument $\Pi_a = J/(aU^2)$ includes a , and represents the effect of the finite size of the source. Π_a can also be interpreted as the ratio of the momentum flux delivered by the forcing to the momentum per unit time transported by the stream through the cross section of the forcing area. Dimensionless frequency $St = fJ/U^3$ can be interpreted as an analogue of the Strouhal number.

Several series of simulations were performed to study the regime of the flow in the space of the two dimensionless control parameters. The results of these simulations are summarized in the diagram in Figure 2. Triangles in Figure 2 indicate a stable regime when no vortex street was observed. Shaded circles indicate the regime when periodic

shedding of vortices was observed and the frequency of shedding was measured. Finally, the regime when the irregular ejection of vortex dipoles was observed rather than periodic shedding of vortices is indicated by squares. Lines 1 and 2 in Figure 2 approximately indicate the boundary between the stable regime and the regime of the periodic shedding. Consider now the characteristics of the flow in these regimes in more detail.

In a stable regime the wake is in the form of a jet-like depression in the velocity field such that it is an almost parallel flow far downstream of the force. Note that for values of Π_a larger than a certain value of order of unity a recirculation in the form of an elongated vortex dipole forms in the near wake. This dipole can be related to the vortex bubble observed in the numerical simulations of steady flows behind the circular cylinder by Fornberg [12, 13]. Those simulations employed a numerical technique which allowed one to simulate steady (but unstable) flows for the Reynolds number (up to 600) well above the value (~ 50) where the instability starts otherwise. It was observed that both the width and the length of the wake bubble increase with the Reynolds number such that both of these dimensions far exceed the diameter of the cylinder. The formation of the dipole will be further discussed in this article in the context of transition between different regimes of vortex shedding for the case of unstable flows.

It is interesting to compare the deficit of the x -component of velocity (u) in the wake with the theoretical solution obtained for the point force in the Oseen approximation. The explicit expression for the steady-state ($t \rightarrow \infty$) distribution of u along the x -axis can be easily obtained from the expression for the stream function given in [14]:

$$u(x, 0) = \frac{J}{4\pi\nu\tilde{x}} \left[1 - \tilde{x} \exp(\tilde{x}) (K_0(|\tilde{x}|) + K_{-1}(|\tilde{x}|)) \right], \quad (2)$$

where $\tilde{x} = Ux/(2\nu)$ and K is the modified Bessel function of the second order. Figure 3 demonstrates the distribution of velocity u along the axis of the flow ($y = 0$) in a numerical simulation with relatively low values of both control parameters ($\Pi_a = 1.1$, $\Pi_v = 75$) and that obtained from the steady-state distribution (2). The differences between the numerical and theoretical solutions are practically negligible both upstream and downstream of the force except in the area within a distance of approximately 7 downstream of the force where the differences are due mainly to the fact that the force in numerical simulations is applied within finite area in contrast to a point singularity in the theoretical solution. The fact that the solutions are very close in the far wake indicates that the vorticity transport due to self induced motion in the wake is negligible compared to that by the uniform stream U and the transport due to viscous diffusion. These assumptions constitute the basis of the approximation used to obtain the theoretical solution and they seem to work well when the control parameters Π_a and Π_v are not very large.

Consider now the unstable case when the periodic shedding of vortices is observed. It is interesting to first consider the initial evolution of the flow after its start-up. Two sequences of images in Figures 4 and 5 illustrate the typical transient behavior of the flows prior to the formation of the regular vortex street. Although the final result is similar in both cases, the initial evolution is different. Flow in Figure 4 ($\Pi_a = 1.7$) is characterized by the formation of an elongated wake which becomes undulated and then transforms into a regular vortex street. The second simulation (Figure 5) was chosen such that the value of $\Pi_a = 2.2$ for the flow is greater than that in the previous case. In this

flow vorticity initially accumulates in the form of a vortex dipole (bubble) while the excess of vorticity generated by the forcing forms the elongated tail (wake) behind the dipole. The dipole becomes unstable and is then shed and translates away from the wake. After this initial strong perturbation a regular alternating vortex shedding establishes in the flow.

Independent of the peculiarities of the transient evolution of the flow regular vortex streets finally form in the wake behind the force. Typical vorticity distributions in the developed vortex streets are depicted in Figure 6 a - d. The patterns of vorticity observed in our simulations are visually similar to those observed previously by other authors in numerical simulations of the flow behind a circular cylinder (e.g. Inoue and Yamazaki [15]) as well as in the laboratory experiments performed in water in three dimensional geometry (e.g. Karasudani and Funakoshi [16]) or in soap films in quasi-two-dimensional geometry (Vorobieff et al. [17]). The shedding frequency f was measured in all of our simulations where the regular shedding was observed. The dimensionless frequency in the form of the Strouhal number defined by expression (1) depends on two control parameters. It is therefore difficult to quantify this function for all values of its arguments. As a first step in this direction we plot the data from all of the experiments in a single graph of St vs. Π_a (Figure 7). One indication of the dependence of St on the second control parameter Π_v is given by the fact that the data collapse well on a single curve for large values of Π_a . Most of the data for large Π_a also correspond to large values of Π_v in our simulations. Thus St is not sensitive to Π_v when Π_v is large and one can characterize this behavior in terms of complete similarity of function Φ for large values of its first argument such that $\Phi(\Pi_v \rightarrow \infty, \Pi_a) = G(\Pi_a)$ where G is a

dimensionless function of one argument. Note that the plot in Figure 7 is in good quantitative agreement with a similar plot of the data obtained in the laboratory experiments (compare with Figure 13 in [5]). Two prominent features of the graph in Figure 7 are the discontinuities of the curve which correspond to transitions between different regimes. In terms of the dimensionless argument Π_a the transition from the stable regime (zero frequencies) to periodic shedding occurs at approximately $\Pi_a = 1.5$. For $\Pi_a \approx 2.65$ the flows undergo further transition which can be identified by a rapid drop in frequency. Let us return to Figure 6 where plates a and b show the flows before the transition while plates c and d show the flow immediately at transition point and after the transition to reduced frequency regime. Visual comparison of the near wakes in plates a, b and c, d demonstrate clear differences in the pattern of vortices. The vortex street before the transition (plates a and b) can be characterized by a relatively small spacing between the vortices in the y direction such that the vortices are located almost at the axis of the flow one after another. In contrast the vortex street after the transition (plates c and d) is of typical staggered pattern and is characterized by a significant spacing in y direction. It is interesting to clarify the nature of this second transition. Close inspection of velocity fields near the origin (Figure 8 a, b) reveals that before the transition, when the velocity of the stream is high and the magnitude of the force is low, the stream prevails and the forcing only creates a region with a depression in the magnitude of the velocity of the stream. In contrast, after the transition when the velocity of the stream is relatively low and the magnitude of the force is high, the forcing creates a region of recirculation (vortex dipole) near the origin such that the velocity at the x-axis within this region is in the opposite direction to that of the stream. The transition can therefore be

identified by the appearance of a stagnation point in front of the force. Thus one can further conclude that the rapid changes in the properties of the instability (drop in frequency) are due to the change in the characteristics of the base flow.

Another interesting phenomenon which is worth mentioning here is the onset of the secondary vortex street in the far wake. Taneda [18] observed in his visualization experiments that vortex streets behind a cylinder break down at some distance from the cylinder and transform into two shear layers. These shear layers then form a new (secondary) vortex street consisting of vortices of larger scale forms farther downstream. The formation of the secondary vortex street is believed to be due to the (2D) instability based on the local mean velocity profile in the far wake as was originally suggested by Taneda rather than due to the vortex pairing of the primary vortex street. Williamson and Prasad [19] who studied three-dimensional effects in the flow concluded that large-scale instability wave in the far wake is 2D even in the presence of 3D effects (oblique shedding in the near wake) and that this large-scale wave cannot possibly be the result of the vortex pairing. Manifestation of the similar effect in the far wake in our purely two-dimensional simulations is in agreement with those conclusions. The downstream position of the onset of the secondary wake was shown to be proportional to $Re^{-1/2}$ (Vorobieff et al. [17]). Although the study of this secondary instability was not the main goal of our simulations, we were able to observe the formation of the secondary vortex street because the computational domain was long enough. Typical examples are shown in Figure 6 c and d.

It is interesting to discuss here if there exists a straightforward relation between the flows generated by a constant (independent on velocity) force as described here and

the flow around a circular cylinder. The flow around a circular cylinder is controlled by three dimensional parameters: the diameter of the cylinder d , the velocity of the stream U and the kinematic viscosity of fluid ν . The force applied by the cylinder on the fluid is not an independent parameter but rather depends on the control parameters of the flow:

$$J = \frac{1}{2} C_D d U^2, \quad (3)$$

where C_D is the drag coefficient [1]. We can then use (3) to relate our dimensionless parameters to those in the problem with the cylinder as follows:

$$St = \frac{1}{2} C_D \frac{fd}{U} = \frac{1}{2} C_D St_c, \quad (4)$$

$$\Pi_a = \frac{1}{2} C_D \frac{d}{a}, \quad (5)$$

$$\Pi_\nu = \frac{1}{2} C_D \frac{dU}{\nu} = \frac{1}{2} C_D Re_c. \quad (6)$$

Here we introduced the Strouhal number, St_c , and the Reynolds number, Re_c , for the flow around the cylinder.

Thus the flows which correspond to those past a circular cylinder should be represented by a line in two-parameter space in the regime diagram (Figure 2). However, an appropriate criterion should be developed in order to identify this line. Herein we offer such a criterion and then compare the main characteristic of the flow with those for the circular cylinder to support the original hypothesis. The following physical arguments can be used to develop the criterion. In the extreme case when the force is very strong and the velocity of the stream is small (or zero), the force generates a starting vortex dipole [3, 4] which continuously propagates forward in the direction of the applied force. In the presence of the incoming stream this flow can be unstable and either regular vortex

shedding or irregular ejection of dipoles occurs. This flow can be identified with the jet intruding into the quiescent fluid rather than with the flow past a cylinder. Another extreme is when the stream prevails and the force is weak. In this case the wake is in the form of a depression in the velocity field and no stagnation point appears in front of the forcing. The only distinct point between these extremes is when the stagnation point first occurs at $\Pi_a \approx 2.65$. It is natural then to choose the line $\Pi_a = 2.65$ (dashed line in Figure 2) as the one representing the flows past a cylinder. To validate this conclusion we have to compare the dimensionless frequency of vortex shedding for the flows on the line with that for a circular cylinder. Since the flows past a cylinder become essentially three-dimensional for the Reynolds number higher than approximately 180, we choose the results of purely two-dimensional calculations for comparison. Barkley and Henderson [20] report the results of their Floquet stability analysis for $Re_c = 50 - 250$. Their results are given in the form St_c vs. Re_c . It is convenient however to use the dimensionless frequency in the form of the Roshko number $Ro = St_c Re_c = fd^2/\nu$ because we can expect a linear dependence on the Reynolds number. Linear fit to data in [20] gives the relation

$$Ro = 0.23(Re_c - 24). \quad (7)$$

To make further progress the dependence of the drag coefficient C_D on the Reynolds number is required in order to relate the parameters Π_a or Π_v to Re_c . Two-dimensional numerical simulations by Henderson [21] supported by experimental results in soap films by Wen et al. [22] give the empirical dependences both for the stable regime as well as for vortex shedding regime up to the Reynolds number 1000. We employed these dependences to calculate both Re_c and C_D for all of our runs from expression (6). The Roshko number was then calculated and plotted for different values of Re_c (Figure 9).

Dots in graph in Figure 9 represent all data for regular vortex shedding while shaded circles show all data in the vicinity (6% interval were chosen somewhat arbitrarily to include more data points) of the line $\Pi_a = 2.65$ in the regime diagram. Solid line in Figure 8 shows dependence (7) and is in good agreement with our data. It would appear that this result shows that our original hypothesis that the flows generated by a force at $\Pi_a = 2.65$ are related to those past a circular cylinder, is valid.

3. CONCLUSION

In summary, it can be concluded that the results of numerical simulations reported in this article provide a detailed description of the behavior of the Strouhal number for different values of control parameters which include the magnitude of the forcing and the velocity of the stream. Two distinct regimes of vortex shedding were observed in our simulations. The transition between regimes is in the form of a rapid drop in frequency. The flow in the first (high frequency) regime when the velocity of the stream is high and the magnitude of the force is low, is characterized by a depression in the magnitude of the velocity of the stream in the vicinity of the source. In contrast the flow in the second (reduced frequency) regime when the forcing is relatively strong, is characterized by the formation of a recirculation region in the form of a vortex dipole. The transition between these regimes is characterized by the appearance of a stagnation point in front of the force. The transition occurs at constant value of $\Pi_a = 2.65$ and which is further recognized as being the location in the parameter space for the flows related to those past a circular cylinder. It can further be concluded in the context of the relation between the

flows generated by a Gaussian distribution of a force and those due to the presence of a solid bluff body that the relation between these flows is not immediately obvious. A method where the force depends on the local velocity [8] provides perhaps a more straightforward way of simulating a bluff body with a force. However, the results described herein demonstrate that the constant force generates a class of flows which are related to many different hydrodynamical phenomena including starting vortex dipoles, jets as well as bluff body wakes. This class of flows is of interest by itself due to these many connections. This approach therefore deserves further attention as it provides a generalized point of view on these flows and their instabilities.

Acknowledgement

The research reported in this paper has been supported by the Natural Sciences and Engineering Research Council of Canada under grants 300805-04 and 227192-04.

References

- [1] M. M. Zdravkovich, *Flow Around Circular Cylinders*, Oxford University Press (1997).
- [2] C. H. K. Williamson and R. Govardhan, Vortex-induced vibrations, *Annu. Rev. Fluid Mech*, **36**, 413–455 (2004).
- [3] S.I. Voropayev, and Y.D. Afanasyev, *Vortex Structures in a Stratified Fluid*, Chapman and Hall, London (1994).

- [4] Y.D. Afanasyev and V.N. Korabel, Starting vortex dipoles in a viscous fluid: asymptotic theory, numerical simulations and laboratory experiments, *Phys Fluids*, **16**, 3850 (2004).
- [5] Y.D. Afanasyev, and V.N. Korabel, Wakes and vortex streets generated by translating force and force doublet: laboratory experiments, *J. Fluid Mech.*, **553**, 119-141 (2006).
- [6] E. A. Gillies, Low-dimensional control of the circular cylinder wake, *J. Fluid Mech.*, **371**, 157-178 (1998).
- [7] P. Reichl, K. Hourigan and M. C. Thompson, Flow past a cylinder close to a free surface, *J. Fluid Mech.*, **533**, 269-296 (2005).
- [8] J. C. Padrino and D. D. Joseph, Numerical study of the steady-state uniform flow past a rotating cylinder, *J. Fluid Mech.*, **557**, 191-223 (2006).
- [9] M.R. Maxey, and B. K. Patel, Localized force representations for particles sedimenting in Stokes flow, *Intern. J. of Multiphase Flow* **27**, 1603 (2001).
- [10] P. Angot, C.-H. Bruneau and P. Fabrie, A penalization method to take into account obstacles in incompressible viscous flows, *Numer. Math.* **81**, 497 (1999).
- [11] M. Braza, P. Chassaing, and H.H. Minh, Numerical study and physical analysis of the pressure and velocity fields in the near wake of a circular cylinder, *J. Fluid Mech.*, **165**, 79-130 (1986).
- [12] B. Fornberg, A numerical study of steady viscous flow past a circular cylinder, *J. Fluid Mech.*, **98**, 819 (1980).
- [13] B. Fornberg, Steady viscous flow past a circular cylinder up to Reynolds number 600, *J. Comput. Phys.*, **61**, 297 (1985).

- [14] Y.D. Afanasyev, Wakes behind towed and self-propelled bodies: asymptotic theory, *Phys Fluids*, **16**, 3235 (2004).
- [15] O. Inoue, T. Yamazaki, Secondary vortex streets in two-dimensional cylinder wakes, *Fluid Dyn. Res.* **25**, 1-18 (1999).
- [16] T. Karasudani, M. Funakoshi, Evolution of a vortex street in far wake of a cylinder, *Fluid Dyn. Res.* **14**, 331 (1994).
- [17] P. Vorobieff, D. Georgiev and M. S. Ingber, Onset of the second wake: Dependence on the Reynolds number, *Phys. Fluids*, **14**, 7 (2002).
- [18] S. Taneda, Downstream development of the wakes behind cylinders, *J. Phys. Soc. Jpn.* **14**, 843 (1959).
- [19] C. H. K. Williamson and A. Prasad, Wave interactions in the far wake of a body, *Phys. Fluids A* **5**, 1854 (1993).
- [20] D. Barkley and R. D. Henderson, Three-dimensional Floquet stability analysis of the wake of a circular cylinder, *J. Fluid Mech.*, **322**, 215 (1996).
- [21] R. D. Henderson, Details of the drag curve near the onset of vortex shedding, *Phys. Fluids*, **7**, 2102 (1995).
- [22] C. -Y. Wen, C. -L. Yeh, M. -J. Wang and C. -Y. Lin, On the drag of two-dimensional flow about a circular cylinder, *Phys. Fluids*, **16**, 3828 (2004).

Figure captions:

Figure 1. Computational grid. The distance is in units of $2a$.

Figure 2. Regime diagram in two-parameter space: stable regime (triangles), regular vortex shedding (shaded circles) and irregular shedding (squares). Solid lines 1 and 2 indicate the boundary between the stable regime and the regime of regular shedding. Dashed line 3 ($\Pi_a = 2.65$) shows the transition between the high and low frequency regimes of the vortex shedding as well as the location of the flows which are related to the flows past a circular cylinder.

Figure 3. Distribution of the x -component of velocity along the axis of the flow ($y = 0$). The theoretical relation (3) is shown by solid lines while symbols show the data obtained in a simulation with control parameters: $\Pi_a = 1.1$, $\Pi_v = 75$.

Figure 4. Sequence of images showing the transient evolution of the flow with control parameters $\Pi_a = 1.7$ and $\Pi_v = 105$: $t = 7.7$ (a), 38 (b), 115 (c) and 208 (d). Vorticity varies from -2.3 to 2.3.

Figure 5. Same as in Figure. 4 but for $\Pi_a = 2.1$ and $\Pi_v = 120$: $t = 29$ (a), 6 (b), 57 (c) and 86 (d).

Figure 6. Contours of vorticity for four simulations with the same free-stream velocities U but different forcing amplitudes: (a) $\Pi_a = 1.4$, (b) $\Pi_a = 2.1$, (c) $\Pi_a = 2.6$, (d) $\Pi_a = 3.2$. Vorticity varies from -4 to 4.

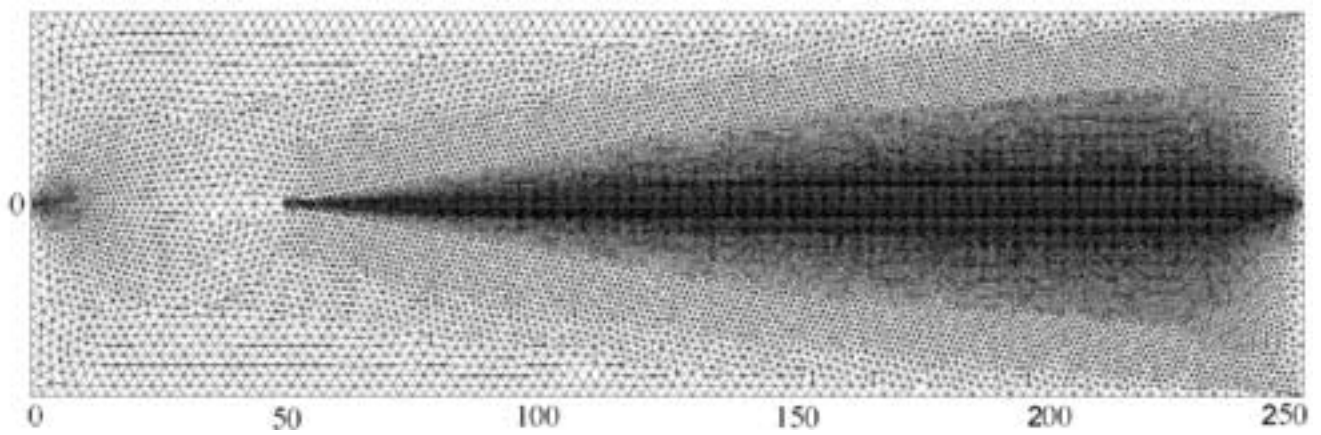
Figure 7. Strouhal number *versus* the dimensionless parameter Π_a . Triangles indicate stable flows (zero frequency) while circles show the regular shedding regime.

Figure 8. Velocity vectors in the vicinity of the origin after the start of the flow for two simulations with the same J but different stream velocities: (a) $\Pi_a = 2.1$ and (b) $\Pi_a = 8.4$.

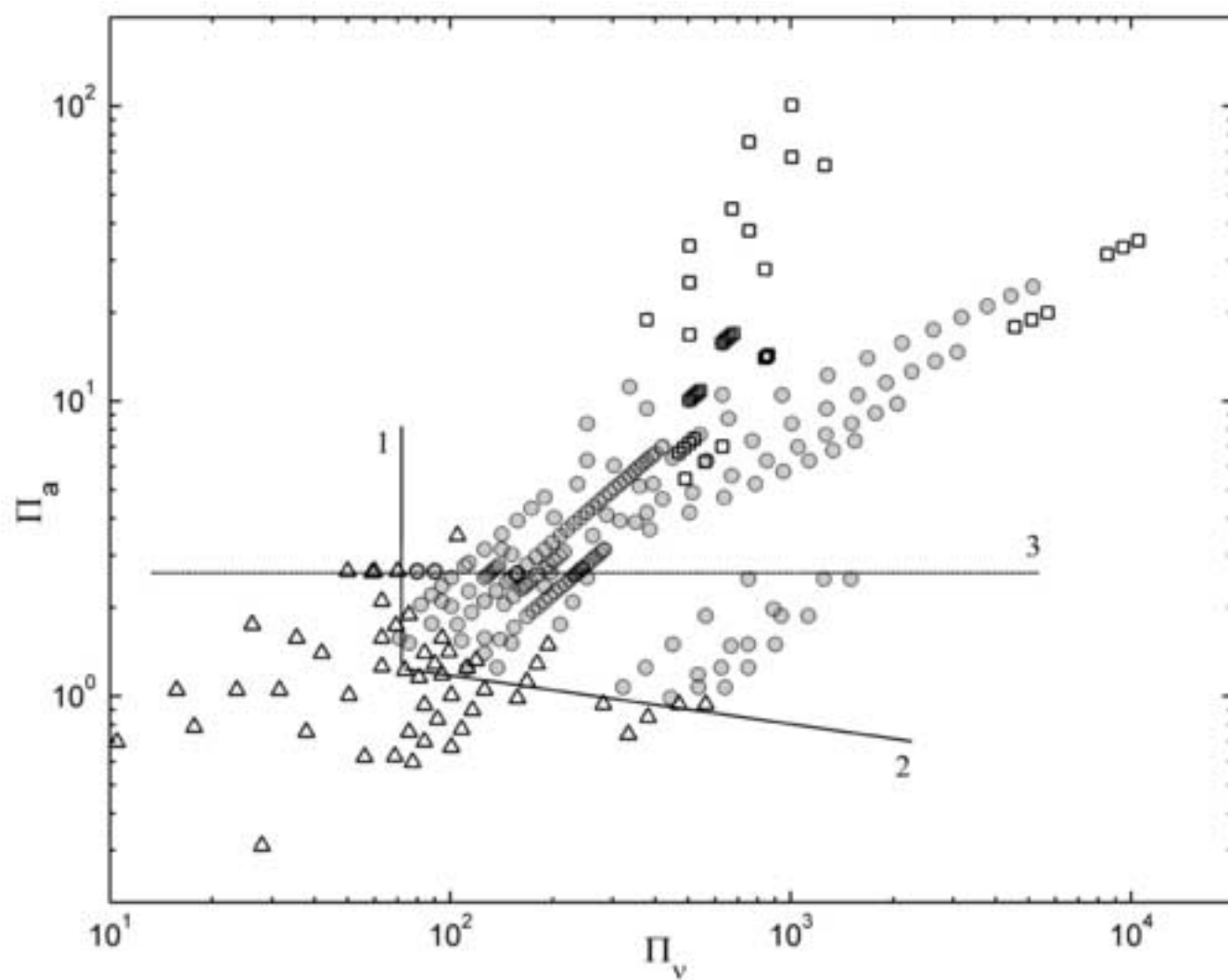
Figure 9. Ro vs. Re_c for all experiments with regular vortex shedding (dots). Circles indicate runs where Π_a is within 6% of the value 2.65. Solid line shows dependence (7) for numerically simulated two-dimensional flows past a circular cylinder [20].

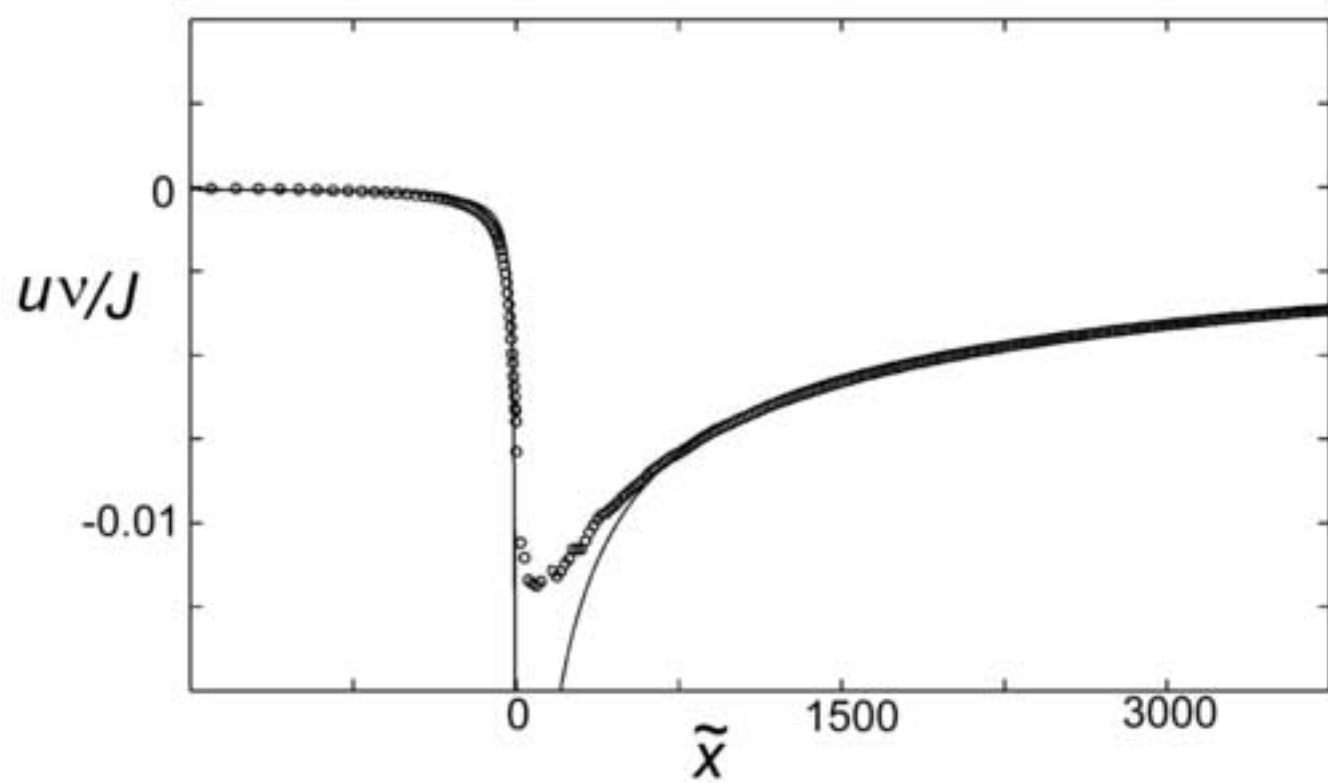
Figure(s)

[Click here to download high resolution image](#)

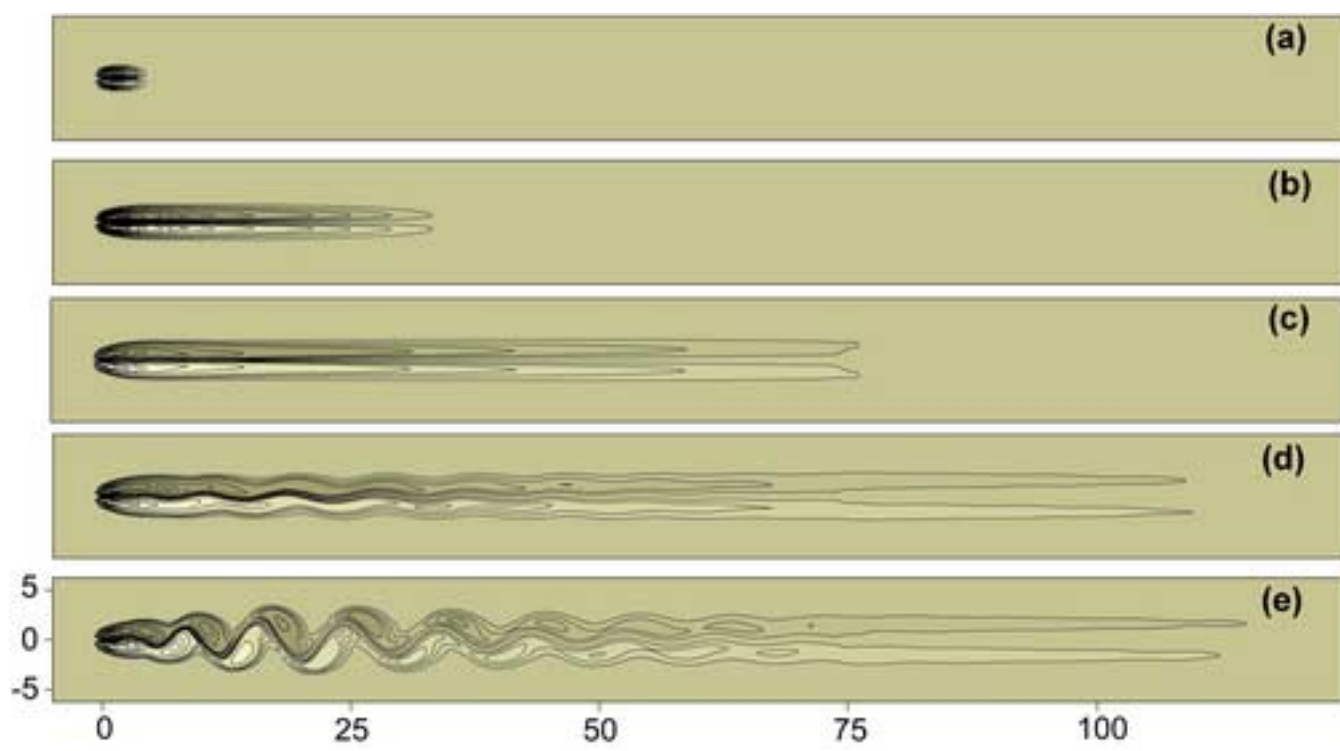


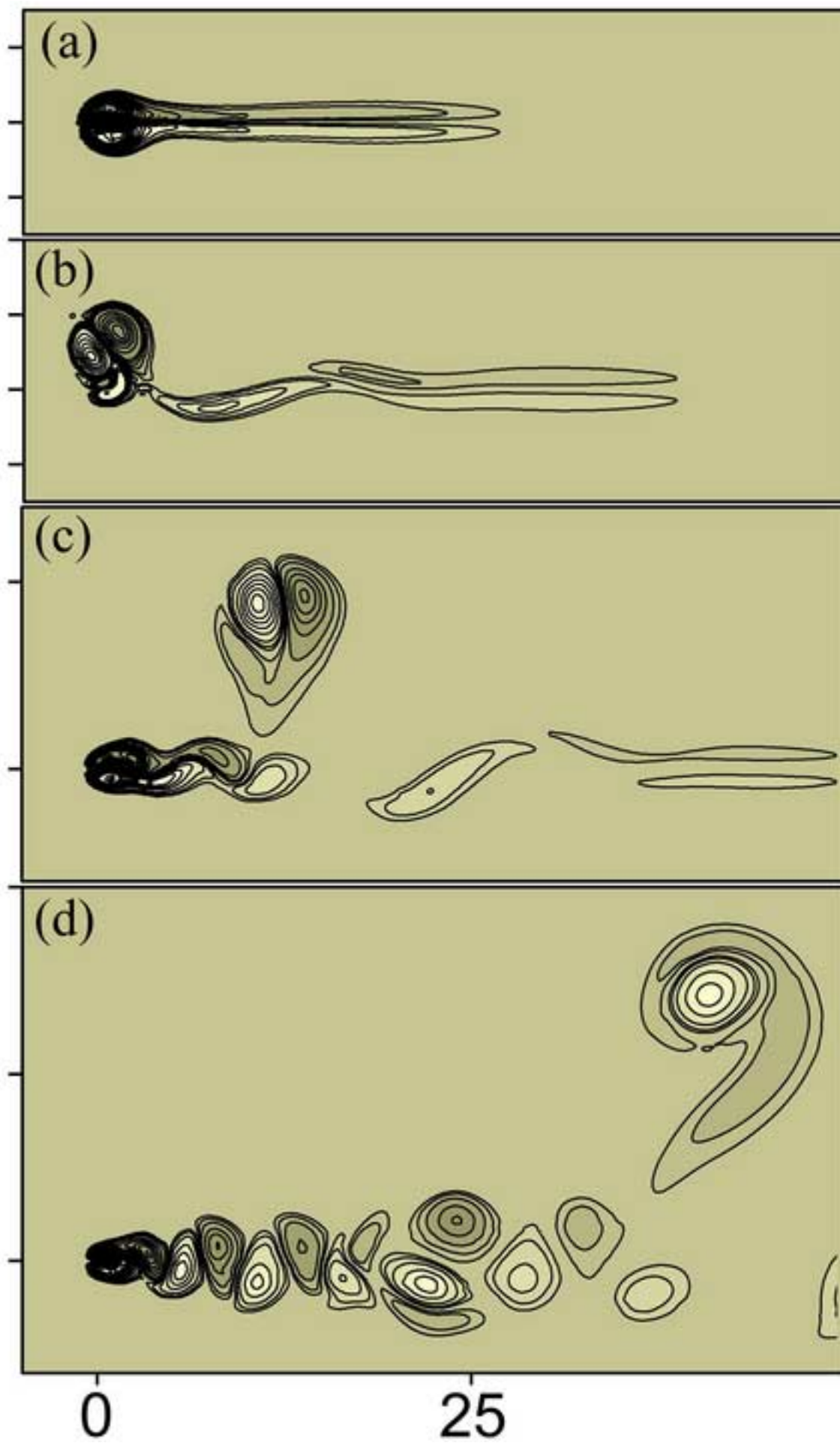
Figure(s)
[Click here to download high resolution image](#)

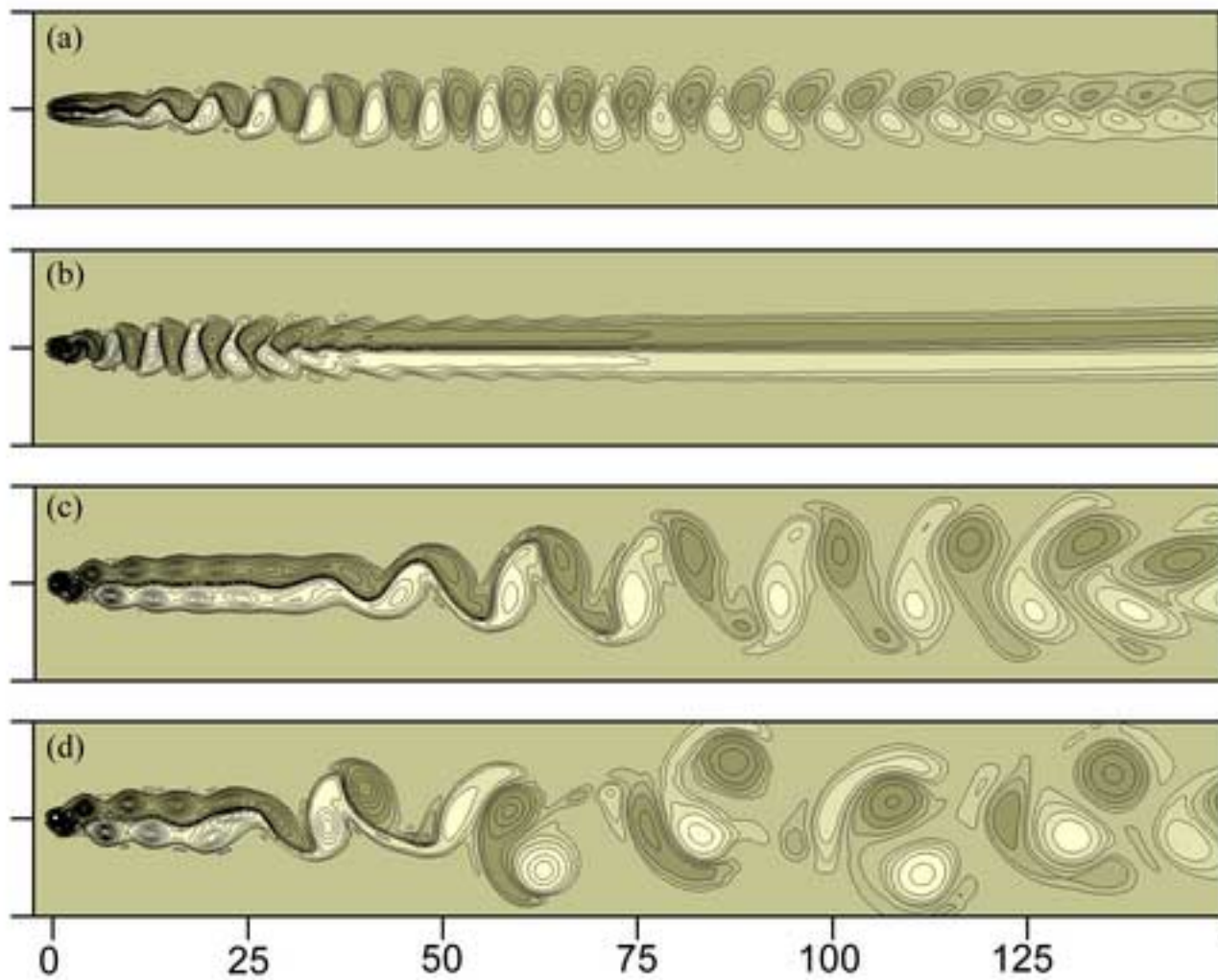




Figure(s)
[Click here to download high resolution image](#)

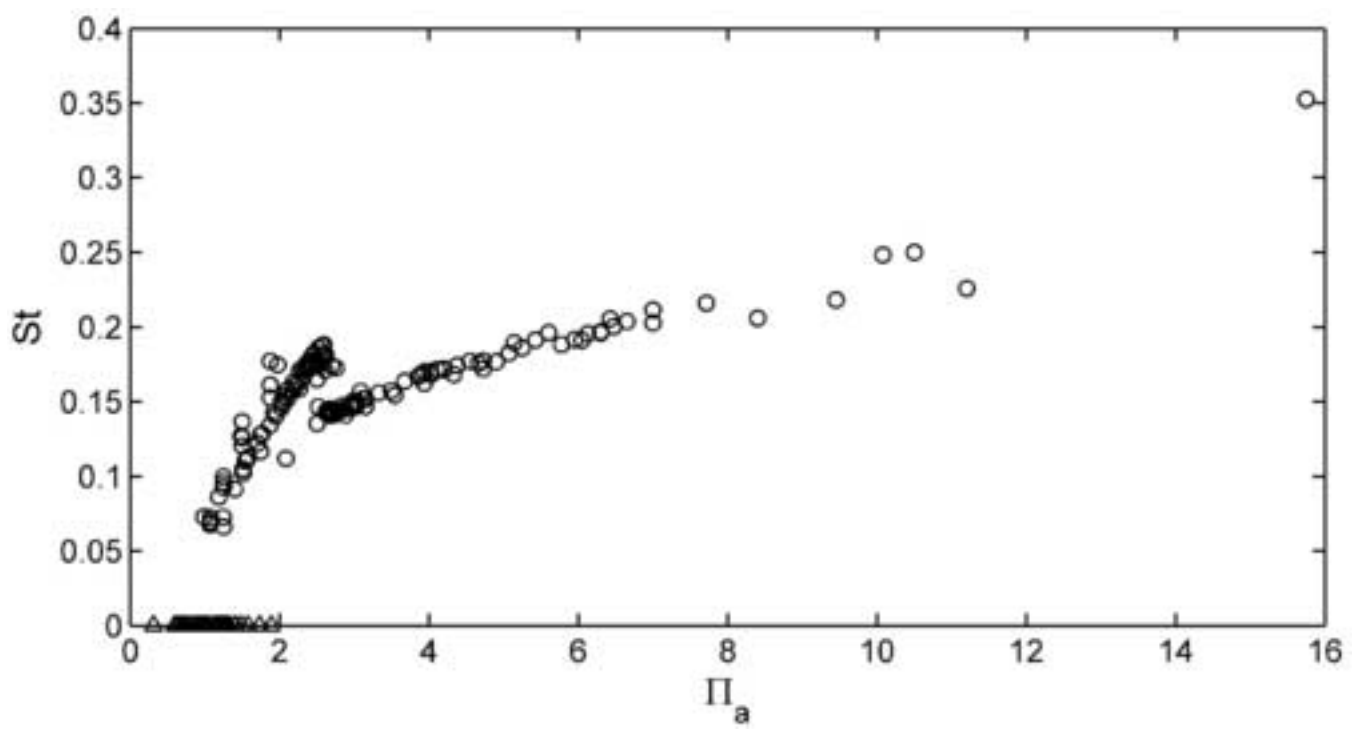




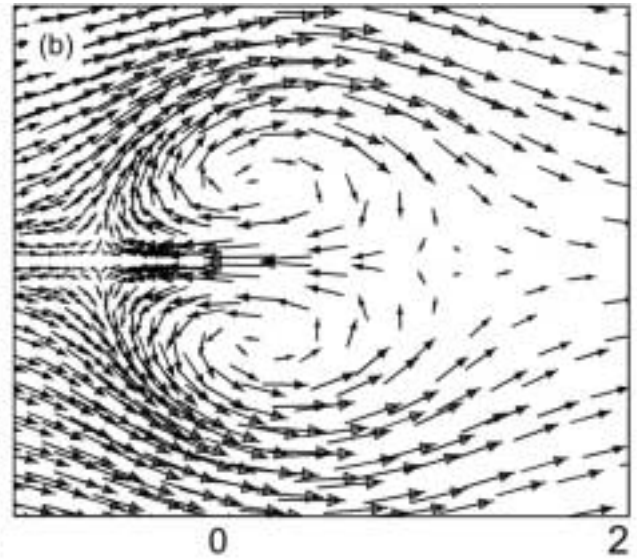
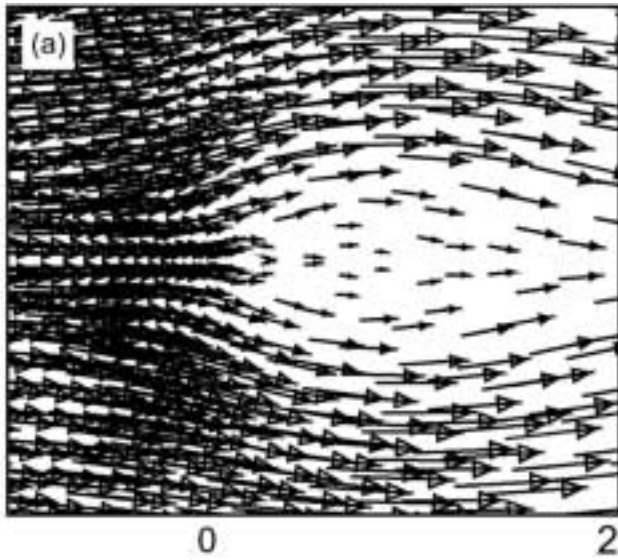


Figure(s)

[Click here to download high resolution image](#)



Figure(s)
[Click here to download high resolution image](#)



Figure(s)
[Click here to download high resolution image](#)

